Coupling of N_2^+ rotational states in an air laser from tunnel-ionized nitrogen molecules

Hongqiang Xie,[1,2] Bin Zeng,[1,*] Guihua Li,[1] Wei Chu,[1] Haisu Zhang,[1] Chenrui Jing,[1,2] Jinping Yao,[1] Jielei Ni,[1] Zhaohui Wang,[1,2] Ziting Li,[1,2] and Ya Cheng[1,†]

[1]*State Key Laboratory of High Field Laser Physics, Shanghai Institute of Optics and Fine Mechanics, Chinese Academy of Sciences, Shanghai 201800, China*

[2]*University of Chinese Academy of Sciences, Beijing 100049, China*

(Received 26 June 2014; published 13 October 2014)

We report on experimental and theoretical investigations of dynamic evolution of individual R-branch laser lines from tunnel-ionized nitrogen molecules based on a pump-probe scheme. Our observation shows that the intensities of the R-branch laser lines exhibit rapid oscillations which can be decomposed into periodic oscillations at different frequencies. The oscillations can be attributed to the coupling between the rotational quantum states mediated either by the probe pulses or by the P-branch laser emission from the molecular ions.

DOI: 10.1103/PhysRevA.90.042504 PACS number(s): 33.20.Sn, 42.50.Hz, 42.65.Re

I. INTRODUCTION

Recently, free-space lasers generated during femtosecond laser filamentation in nitrogen gas have attracted considerable attention [1–5]. The nitrogen lasers not only provide new opportunities for remote sensing in ambient air, but also extend the territory of strong field molecular physics [6–8]. In general, the nitrogen lasers can be categorized into two groups, i.e., one operated at 337-nm wavelength (corresponding to $C^3\Pi_u \rightarrow B^3\Pi_g$ transition) in neutral molecules and the other operated at wavelengths such as 391 nm, 428 nm, etc. (corresponding to $B^2\Sigma_u^+ \rightarrow X^2\Sigma_g^+$ transitions) in nitrogen molecular ions. So far, the pumping mechanism of the molecular nitrogen lasers at 337 nm has been identified, which is attributed to the collisional excitation between electrons and molecules [9,10], whereas the mechanism behind the molecular ion laser of nitrogen is still under hot debate. Several models have been proposed to interpret the physics of such air lasers, including stimulated emission based on seed amplification in a population-inverted system, four-wave mixing, and seed-triggered super-radiance, etc. [11–15]. In particular, Kartashov *et al.* recently proposed that the different rotational periods of aligned molecular ions on the ground and excited electronic states can lead to transient laser gain and thus the creation of bright narrow-bandwidth coherent UV emissions in suitable time windows [15]. Nevertheless, these models have been neither deterministically confirmed nor widely accepted.

Recently, Zhang *et al.* observed that the rotational coherence of the molecular ions can encode its characteristics into the air laser [16]. The coherent rotational wave packet of the molecular ions was achieved either by ionization-induced alignment [17] or by Raman-type interaction of the pump laser with the molecules [18], or a combination of the two. Motivated by this finding, Zeng *et al.* further investigated the ultrafast dynamics of the rotational coupling in the lasing action by carrying out frequency-resolved pump-probe measurements of the laser lines corresponding to R-branch transitions ($\Delta J = -1$) and discovered that the laser lines show a fast oscillation [19] which can be ascribed to the quantum beat between two adjacent rotational states $|J\rangle$ and $|J+2\rangle$ in the rotational wave packet. In the current work, we carry out a more systematic investigation of the unusual behavior in the pump-probe measurement of the individual laser lines corresponding to R-branch transitions ($\Delta J = -1$) and analyze the result by theoretical simulations. Specifically, we show that at high pump laser intensities, the evolution of the laser signal from an individual rotational state J can show complex behaviors due to the contribution from the coupling of the rotational states which are far away from the rotational states of J, J-2, and J+2. Our analysis reveals that the probe pulses act as not only a seed that triggers the stimulated amplification, but also a redistributor of rotational sates of the molecular wave packet initially aligned by the intense pump pulses.

II. EXPERIMENTAL SETUP

The pump-probe experimental setup is shown in Fig. 1. The femtosecond laser pulses (1 kHz, 800 nm, ~40 fs) from a commercial Ti:sapphire laser system (Legend Elite-Duo, Coherent, Inc.) were split into two paths with a 50% beam splitter. The first beam serving as the pump was focused by a 30-cm focal-length lens into a vacuum chamber filled with nitrogen gas at a pressure of 3 mbar to align and ionize the nitrogen molecules. The other beam, after being frequency doubled by a 0.2-mm-thick β-barium borate crystal, was used as the probe to stimulate the coherent laser emissions. A Glan-Taylor prism was put in the probe-beam path to ensure that the probe pulse was linearly polarized. Besides, a half wave plate was inserted in the pump-beam path to control the polarization direction of the pump pulse, which was set to be parallel to that of the probe pulse in our experiment. The time delay between the pump and probe pulse was controlled by a motorized linear transitional stage with a temporal resolution of 16.7 fs. The generated coherent emissions were collimated by a 30-cm focal-length lens and then recorded by a 1200-grooves/mm grating spectrometer (Andor Shamrock 303i) with a spectral resolution of 0.06 nm.

III. EXPERIMENTAL RESULTS

We first examine the laser emission at 391 nm [i.e., $B^2\Sigma_u^+(\upsilon = 0) \rightarrow X^2\Sigma_g^+(\upsilon = 0)$] generated by collinearly

*bzeng@foxmail.com
†ya.cheng@siom.ac.cn

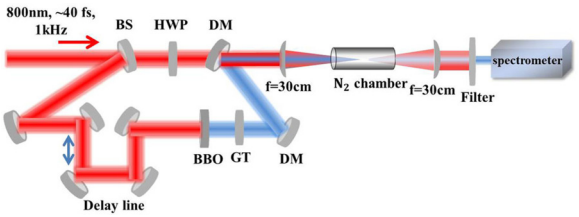

FIG. 1. (Color online) Schematic diagram of the experimental setup. BS: beam splitter; GT: Glan-Taylor prism; DM: dichroic mirror with high reflectivity at ~400 nm and high transmission at ~800 nm; HWP: broadband half wave plate at ~800 nm; filter: neutral density filter.

focusing a 2-mJ, 800-nm pump pulse and a time-delayed 400-nm probe pulse into the gas chamber containing 3 mbar nitrogen gas. The results are shown in Fig. 2, which is consistent with our previous observation [19]. Figure 2(a) is a typical forward lasing spectrum and the inset is a close-up view of R-branch lasing lines (indicated in the box) from the individual rotational quantum number J labeled on each peak. The R-branch lasing intensities from the individual rotational state J as a function of the time delay between the pump and the probe pulses are plotted in Fig. 2(b), in which a fast oscillation and a slow oscillation are clearly observed. Figure 2(c) shows the Fourier transforms of the curves in Fig. 2(b). We can see that the frequencies of the fast oscillations increase with the increasing rotational quantum number J, as indicated by the red dashed line, which can be well reproduced by the equation $\Omega_B = (4J-2)B_Bc$, where B_B is the rotational constant of the electronic states $B^2\Sigma_u^+$ of N_2^+. There are also other frequencies $\Omega_X = (4J+2)B_Xc$, as indicated by the black dash-dotted line in Fig. 2(c), where B_X is the rotational constant of the electronic states $X^2\Sigma_g^+$ of N_2^+.

When the pump energy was increased to 2.4 mJ, the R-branch lines of the nitrogen ion laser originating from multiple J states can be observed with the highest rotational quantum number $J = 29$, as shown in Fig. 3(a). From Fig. 3(b), we can see that besides the frequency $(4J-2)B_Bc$, more frequency components such as $(4J-10)B_Bc$ and $(4J+6)B_Bc$ appear in the time-dependent lasing lines of

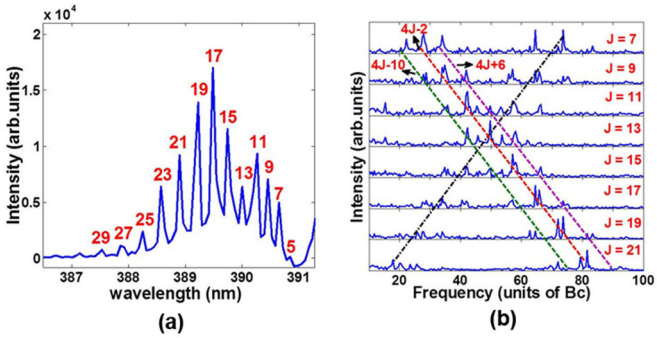

FIG. 3. (Color online) (a) The forward lasing spectrum of R-branch transitions at a pump energy of 2.4 mJ. (b) The Fourier transforms of time-dependent lasing intensities of R-branch transitions.

the individual rotational state J. Surprisingly, Fig. 3(b) also shows an unexpected difference compared with the result in Fig. 2(c). For each individual rotational state J, the lasing emission intensities are modulated not only at the frequency $(4J-2)B_Bc$ which increases linearly with increasing J as indicated by the red dashed line, but also at a new frequency which decreases linearly with the increasing J value, as indicated by the black dash-dotted line. The red dashed and black dash-dotted lines form an "X" structure in the Fourier transform spectrum. We find that the two arms of the "X" structure can be well fitted with the expressions $(4J-2)B_Bc$ and $[4\times(26-J)-2]B_Bc$. In the following, we discuss the physics behind the "X" structure.

IV. THEORETICAL ANALYSIS AND DISCUSSION

For a diatomic molecule, an eigenstate of the molecule in a field-free condition can be denoted as $|J_i, M_i\rangle$, where J is the rotational angular momentum and M is its projection onto the z axis. When the pump 800-nm pulse interacts with the molecule, the initial state $|J_i, M_i\rangle$ will evolve into the superposition of a series of coherent states$|J', M_i\rangle$, which can be expressed with a general form as follows:

$$|\Psi(t)\rangle = \sum_{J'} A_{J'} e^{i\phi_{J'}} e^{-iE_{J'}t} |J', M_i\rangle, \qquad (1)$$

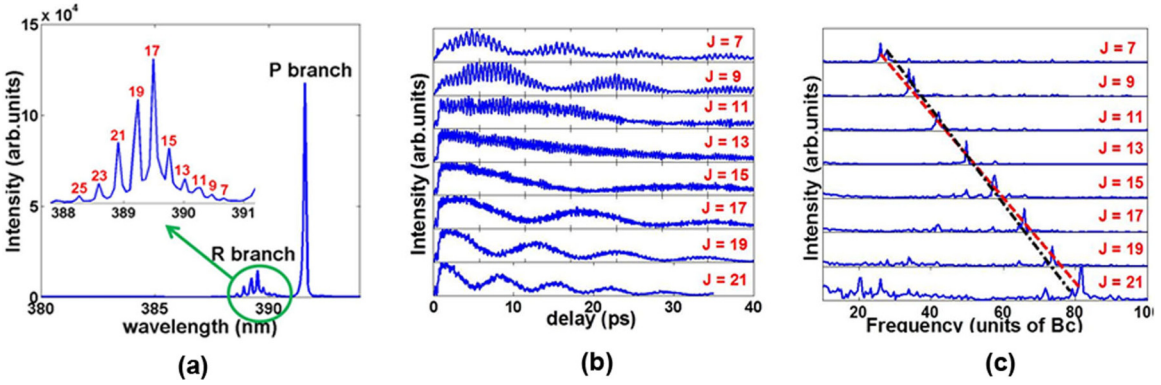

FIG. 2. (Color online) (a) A typical forward lasing spectrum based on the pump-probe configuration. The inset is a close-up view of the R-branch transition, and the numbers label the rotational levels of molecular ions on the excited state. (b) The lasing intensities of each individual rotational state J of the R branch as a function of time delay between the pump and probe pulses. (c) The Fourier transforms of the corresponding curves in (b).

where $A_{J'}$ and $\phi_{J'}$ are the amplitude and the phase of the transition from $|J_i,M_i\rangle$ to $|J',M_i\rangle$, $E_{J'}$ is the eigenenergy of the state $|J',M_i\rangle$, and t denotes the time after the interaction of the molecules with the 800-nm pump pulse.

Later on, upon the arrival of the probe pulse, the state $|J',M_i\rangle$ will experience a transition to the final state $|J,M_i\rangle$ after interacting with the 400-nm probe pulse, and the modulated rotational wave packet can be expressed as [20–22]

$$|\Psi(t)\rangle = \sum_J P_{J,J_i}(\tau)e^{-iE_J(t-\tau)}|J,M_i\rangle, \tag{2}$$

$$P_{J,J_i}(\tau) = \sum_{J'} B_{J'}e^{i\varphi_{J'}}e^{-iE_{J'}\tau}A_{J'}e^{i\phi_{J'}}, \tag{3}$$

where τ denotes the time delay between the 400-nm probe pulse and the 800-nm pump pulse, $B_{J'}$ and $\varphi_{J'}$ are the amplitude and the phase of the transition from $|J',M_i\rangle$ to $|J,M_i\rangle$ induced by the 400-nm pulse. The population of the rotational eigenstate for $|J,M_i\rangle$ after the interaction corresponds to $|P_{J,J_i}(\tau)|^2$:

$$\left|P_{J,J_i}(\tau)\right|^2 = \sum_{J',J''} A_{J'}A_{J''}B_{J'}B_{J''} \times \cos[(E_{J'}-E_{J''})\tau + \phi_{J',J''} + \varphi_{J',J''}]. \tag{4}$$

From Eq. (4), we can learn that the final state $|J,M_i\rangle$ originated from different intermediate states $|J',M_i\rangle$ and $|J'',M_i\rangle$ and has a phase difference $\Delta_{J',J''} = (E_{J'}-E_{J''})\tau + \phi_{J',J''} + \varphi_{J',J''}$; thus these two channels will interfere with each other. In our experiments, the intensity of the 400-nm pulse is very low; hence the high-order rotational couplings such as $|J\rangle \leftrightarrow |J+4\rangle$ can be ignored and only the rotational couplings of $|J\rangle \leftrightarrow |J+2\rangle$ and $|J\rangle \leftrightarrow |J-2\rangle$ need to be taken into consideration. Thus we have

$$\left|P_{J,J_i}(\tau)\right|^2 = \sum_n A_J A_{J+2n} B_J B_{J+2n} \times \cos(\Delta\omega_{J,J+2n}\tau + \phi_{J,J+2n} + \varphi_{J,J+2n}), \quad n = 0, \pm 1, \tag{5}$$

where $\Delta\omega_{J,J+2n} = E_J - E_{J+2n}$, $\phi_{J,J+2n} = \phi_J - \phi_{J+2n}$, and $\varphi_{J,J+2n} = \varphi_J - \varphi_{J+2n}$. The physical meaning of $|P_{J,J_i}(\tau)|^2$ is the probability or the population of molecules at the eigenstate $|J,M_i\rangle$.

For an ensemble of molecules, the probability with which molecules stay at the eigenstate $|J\rangle$ should be addressed by taking into account the thermal distribution,

$$P_J(\tau) = \sum_{J_i}\rho_{J_i}\sum_{M_i=-J_i}^{J_i}\left|P_{J,J_i}(\tau)\right|^2_{M_i}, \tag{6}$$

where ρ_{J_i} accounts for the Boltzmann weights.

The above interference can also be understood through the rotational couplings in the rotational wave packet. As illustrated in Fig. 4(a), the $B^2\Sigma_u^+|J\rangle$ state will experience a transition to the $B^2\Sigma_u^+|J+2\rangle$ state by emitting a P-branch photon and then absorbing an R-branch photon through a resonant Raman process after interacting with the 400-nm pulse. The transition probability from $|J\rangle$ state to $|J+2\rangle$ state can thus be written as

$$P^B_{J,J+2} \propto \cos\left(\Delta\omega^B_{J,J+2}\tau\right). \tag{7}$$

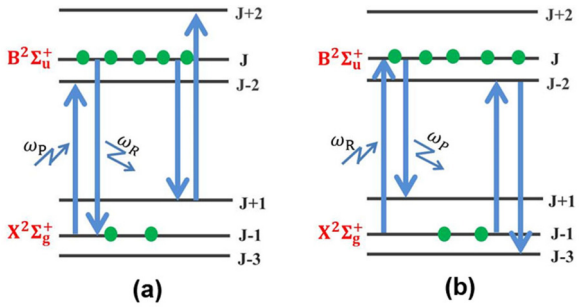

FIG. 4. (Color online) The mechanisms of the modulations in the populations (a) in the rotational level J of the excited state $B^2\Sigma_u^+$ and (b) in the rotational level $J-1$ of the ground state $X^2\Sigma_g^+$.

From Eq. (7), we can see that by changing the time delay between the two pulses, the transition probability, and thus the probability of the molecule staying at $|J\rangle$ state, will vary with the time delay at a frequency of $\Delta\omega^B_{J,J+2} = (4J+6)B_Bc$. On the other hand, since the $|J\rangle$ state can also experience a transition to the $|J-2\rangle$ state by emitting an R-branch photon and absorbing a P-branch photon, the transition probability from the $|J\rangle$ state to the $|J-2\rangle$ state will vary with the time delay between the two pulses at a frequency of $\Delta\omega^B_{J,J-2} = (4J-2)B_Bc$. Therefore the population of nitrogen ions on the excited state can be expressed as

$$N^B_J \propto \sum a_n \cos\left(\Delta\omega^B_{J,J+2n}\tau\right). \tag{8}$$

Since the lasing action relies not only on the population of nitrogen ions on the excited state but also on that of nitrogen ions on the ground state, a modulation in the population of nitrogen ions on the ground state as a function of pump-probe delay will also be reflected in the measured R-branch lasing lines. Likewise, the modulation of the population of nitrogen ions on the ground state can be expressed as

$$P^X_J \propto \sum b_n \cos\left(\Delta\omega^X_{J,J+2n}\tau\right). \tag{9}$$

The population of $X^2\Sigma_g^+|J-1\rangle$ state will show a modulation at the frequency of $\Delta\omega^X_{J-1,J+1} = (4J+2)B_Xc$ due to the coupling of $|J-1\rangle \leftrightarrow |J+1\rangle$ and at the frequency of $\Delta\omega^X_{J-1,J-3} = (4J-6)B_Xc$ due to the coupling of $|J-3\rangle \leftrightarrow |J-1\rangle$, as depicted in Fig. 4(b).

Since the R-branch lasing lines are produced via the transitions corresponding to $B^2\Sigma_u^+|J\rangle \rightarrow X^2\Sigma_g^+|J-1\rangle$, the intensity of an individual R-branch lasing line is determined by the population difference between the excited state $B^2\Sigma_u^+|J\rangle$ and the ground state $X^2\Sigma_g^+|J-1\rangle$ (i.e., the population inversion), which can be written as

$$\Delta N = N_B - N_X \propto \sum_n a_n \cos\left(\Delta\omega^B_{J,J+2n}\tau\right) - \sum_{n'} b_{n'} \cos\left(\Delta\omega^X_{J-1,J-1+2n'}\tau\right). \tag{10}$$

Hence the intensity of the R-branch laser lines will vary not only at the frequencies of $(4J-2)B_Bc$ and $(4J+6)B_Bc$ because of the population modulation of the excited state

$B^2\Sigma_u^+|J\rangle$, but also at the frequencies of $(4J+2)B_Xc$ and $(4J-6)B_Xc$ due to the population modulation of the ground state $X^2\Sigma_g^+|J-1\rangle$. It is noteworthy that in Fig. 2 the lasing intensity of each rotational state is primarily modulated at the frequency components $(4J-2)B_Bc$ and $(4J+2)B_Xc$. Indeed, weak modulations at the frequency components $(4J+6)B_Bc$ and $(4J-6)B_Xc$ can also be observed in Fig. 3(b) when the pump energy is set at 2.4 mJ. For nitrogen ions, the rotational constants of the $B^2\Sigma_u^+$ state and $X^2\Sigma_g^+$ state are $B_B = 2.073\ \text{cm}^{-1}$ and $B_X = 1.92\ \text{cm}^{-1}$ [23]. Since the upper state $B^2\Sigma_u^+$ and the lower state $X^2\Sigma_g^+$ are coherently populated, slow oscillations at the beating frequency of $|(4J-2)B_Bc - (4J+2)B_Xc|$ can be observed in the time domain, as shown in Fig. 2(b).

Remarkably, at the higher pump laser energy of 2.4 mJ, an unexpected oscillation at the frequency component $[4\times(26-J)-2]B_Bc$ clearly appears in Fig. 3(b). The phenomenon suggests existence of efficient coupling between $|J\rangle$ and $|26-J\rangle$ states. We explain the physical mechanism of such coupling as follows. First of all, we notice that at the high pump laser intensity of 2.4 mJ, the R-branch lasing lines originating from the rotational states of large quantum numbers J ($J > 13$) and small quantum numbers J ($J < 13$) are of comparable intensities, as evidenced in Fig. 3(a). Secondly, the energy of the P-branch photon can be expressed as [24]

$$E_P(J) = \Delta E_{el} + J(J+1)B_Bc - (J+1)(J+2)B_Xc, \quad (11)$$

where ΔE_{el} is the electronic energy difference between the $B^2\Sigma_u^+(v=0)$ state and $X^2\Sigma_g^+(v=0)$ state. The wavelengths of the P-branch photons as a function of the rotational quantum number J are plotted in Fig. 5(a). We can see that a band head forms at $J = 13$ because of the relationship $B_X < B_B$. Since the P-branch photons from J and 26-J states have almost the same energy, these photons are essentially indistinguishable.

Recall that in the resonant Raman scattering $|J\rangle \leftrightarrow |J+2\rangle$ induced by 400-nm pulses, an R-branch photon and a P-branch photon must be involved in the couplings of $|J\rangle \leftrightarrow |J+2\rangle$ and $|26-J\rangle \leftrightarrow |28-J\rangle$, as schematically illustrated in Fig. 5(b). Therefore the population of the $B^2\Sigma_u^+|J\rangle$ state N_J is affected by the coupling of $|J\rangle \leftrightarrow |J+2\rangle$, which is proportional to the total number of P-branch photons $n^P_{J,J+1}$. As stated above, the P-branch photons from J and 26-J states are indistinguishable because of their same photon energy. Therefore, the P-branch photon number $n^P_{J,J+1}$ will be affected by the coupling of $|26-J\rangle \leftrightarrow |28-J\rangle$, which is related to the population of the $B^2\Sigma_u^+|26-J\rangle$ state. The time-varying P-branch photon number will leave its signature in the population of the $B^2\Sigma_u^+|J\rangle$ state, namely, the oscillation at the frequency of $[4\times(26-J)-2]B_Bc$, as indicated by the black dash-dotted line in Fig. 3(b). Likewise, the population of $B^2\Sigma_u^+|26-J\rangle$ will also be affected by $B^2\Sigma_u^+|J\rangle$ mediated by the same P-branch photons. Thus the population of the $B^2\Sigma_u^+|26-J\rangle$ state will vary at a frequency of $(4J-2)B_Bc$.

The validity of the above discussion depends on the fact that P-branch photons from J and 26-J states are spectrally overlapping and indistinguishable. As the wavelength difference of the P-branch photons from J and 26-J states is less than 0.006 nm for all the J numbers, it is impossible to directly separate these photons from their spectra because of the limited resolution of our spectrometer (~0.06 nm). In fact, there exist several spectrum-broadening mechanisms in plasma, such as the thermal Doppler broadening, collisional broadening, Stark broadening, and so on [25,26]. Estimation of the broadened linewidth based on these effects is extremely difficult due to the lack of precise knowledge of many important parameters, such as the plasma density, plasma temperature, strength of the laser field, etc. Therefore we take a different approach to make a qualitative estimation of the linewidth of each P-branch line. In our previous work [19], we have measured the P-branch intensity as a function of the time delay between the 800-nm pump pulse and the 400-nm probe pulse. The linewidth of the P-branch lines can be estimated by performing a Fourier transform of the curve measured in the time domain. [See Figs. 2(a) and 2(b) in Ref. [19].] The calculated linewidth is on the order of 0.02 nm, which is much larger than the spacing between the wavelengths of P-branch photons from J and 26-J states (i.e., 0.006 nm, as mentioned above). Thus we can safely conclude that the P-branch photons from J and 26-J states are indeed spectrally overlapping and essentially indistinguishable.

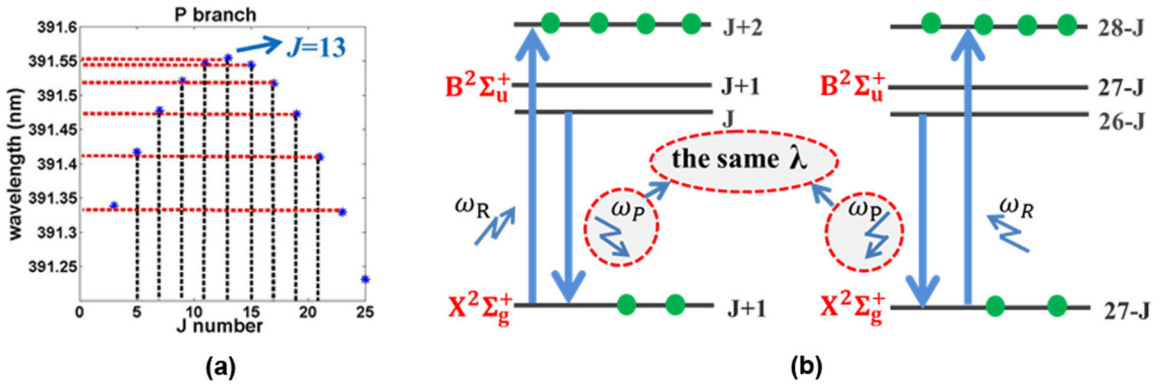

FIG. 5. (Color online) (a) The formation of a bandhead centered at $J = 13$ of P-branch transitions of N_2^+ [$B^2\Sigma_u^+(v=0) \rightarrow X^2\Sigma_g^+(v=0)$]. (b) Schematic illustrations of the resonant Raman coupling processes of $|J\rangle \leftrightarrow |J+2\rangle$ and $|26-J\rangle \leftrightarrow |28-J\rangle$. The P-branch photon of the same photon energy involved in both the processes is indicated with the arrows.

V. CONCLUSION

In conclusion, the R-branch laser emissions originating from $B^2\Sigma_u^+(\upsilon = 0) \rightarrow X^2\Sigma_g^+(\upsilon = 0)$ of nitrogen ions are investigated based on pump-probe measurements. Because of the different pump-pulse intensities used, the rotational state distributions have been found, leading to different rotational state coupling behaviors. At the low pump laser intensity, coupling of $|J\rangle \leftrightarrow |J-2\rangle$ states dominates, whereas at the high pump intensities, couplings between other rotational states, such as $|J-4\rangle \leftrightarrow |J-2\rangle$,$|J\rangle \leftrightarrow |J+2\rangle$ and $|26-J\rangle \leftrightarrow |28-J\rangle$, have been observed. Our findings indicate that the air laser spectroscopy benefits the understanding of the rich physics behind molecular alignment in intense laser fields and molecular rotational coupling mediated by resonant ultrafast laser fields. Meanwhile, the findings also shed new light on the free-space nitrogen ion lasers generated in strong laser fields.

ACKNOWLEDGMENTS

This work was supported by the National Basic Research Program of China (Grants No. 2011CB808100 and No. 2014CB921300), the National Natural Science Foundation of China (Grants No. 11127901, No. 11134010, No. 11204332, and No. 11304330), and the Shanghai "Yang Fan" program (Grant No. 14YF1406100).

[1] Q. Luo, W. Liu, and S. L. Chin, Appl. Phys. B **76**, 337 (2003).
[2] J. Yao, B. Zeng, H. Xu, G. Li, W. Chu, J. Ni, H. Zhang, S. L. Chin, Y. Cheng, and Z. Xu, Phys. Rev. A **84**, 051802 (2011).
[3] D. Kartashov, S. Ališauskas, G. Andriukaitis, A. Pugžlys, M. Shneider, A. Zheltikov, S. L. Chin, and A. Baltuška, Phys. Rev. A **86**, 033831 (2012).
[4] Y. Liu, Y. Brelet, G. Point, A. Houard, and A. Mysyrowicz, Opt. Express **21**, 22791 (2013).
[5] G. Point, Y. Liu, Y. Brelet, S. Mitryukovskiy, P. Ding, A. Houard, and A. Mysyrowicz, Opt. Lett. **39**, 1725 (2014).
[6] C. Jing, H. Zhang, W. Chu, H. Xie, J. Ni, B. Zeng, G. Li, J. Yao, H. Xu, Y. Cheng, and Z. Xu, Opt. Express **22**, 3151 (2014).
[7] J. Ni, W. Chu, H. Zhang, B. Zeng, J. Yao, L. Qiao, G. Li, C. Jing, H. Xie, H. Xu, Y. Cheng, and Z. Xu, Opt. Lett. **39**, 2250 (2014).
[8] S. Hosseini, A. Azarm, J.-F. Daigle, Y. Kamali, and S. L. Chin. Opt. Commun. **316**, 61 (2014).
[9] M. N. Shneider, A. Baltuška, and A. M. Zheltikov, J. Appl. Phys. **110**, 083112 (2011).
[10] S. Mitryukovskiy, Y. Liu, P. Ding, A. Houard, and A. Mysyrowicz, Opt. Express **22**, 12750 (2014).
[11] S. L. Chin, H. Xu, Y. Cheng, Z. Xu, and K. Yamanouchi, Chin. Opt. Lett. **11**, 013201 (2013).
[12] G. Andriukaitis, J. Möhring, D. Kartashov, A. Pugžlys, A. Zheltikov, M. Motzkus, and A. Baltuška, EPJ Web Conf. **41**, 10004 (2013).
[13] G. Li, C. Jing, B. Zeng, H. Xie, J. Yao, W. Chu, J. Ni, H. Zhang, H. Xu, Y. Cheng, and Z. Xu, Phys. Rev. A **89**, 033833 (2014).
[14] J. Ni, W. Chu, C. Jing, H. Zhang, B. Zeng, J. Yao, G. Li, H. Xie, C. Zhang, H. Xu, S. L. Chin, Y. Cheng, and Z. Xu, Opt. Express **21**, 8746 (2013).
[15] A. Baltuska and D. Kartashov, in *Research in Optical Sciences*, OSA Technical Digest (online) (Optical Society of America, Messe Berlin, Berlin, 2014), p. HTh4B.5.
[16] H. Zhang, C. Jing, J. Yao, G. Li, B. Zeng, W. Chu, J. Ni, H. Xie, H. Xu, S. L. Chin, K. Yamanouchi, Y. Cheng, and Z. Xu, Phys. Rev. X **3**, 041009 (2013).
[17] D. Pavicic, K. F. Lee, D. M. Rayner, P. B. Corkum, and D. M. Villeneuve, Phys. Rev. Lett. **98**, 243001 (2007).
[18] T. Seideman and E. Hamilton, Adv. At. Mol. Opt. Phys. **52**, 289 (2005)
[19] B. Zeng, W. Chu, G. Li, J. Yao, H. Zhang, J. Ni, C. Jing, H. Xie, and Y. Cheng, Phys. Rev. A **89**, 042508 (2014).
[20] J. Yao, G. Li, X. Jia, X. Hao, B. Zeng, C. Jing, W. Chu, J. Ni, H. Zhang, H. Xie, C. Zhang, Z. Zhao, J. Chen, X. Liu, Y. Cheng, and Z. Xu, Phys. Rev. Lett. **111**, 133001 (2013).
[21] H. Hasegawa and Y. Ohshima, Phys. Rev. Lett. **101**, 053002 (2008).
[22] A. S. Meijer, Y. Zhang, D. H. Parker, W. J. van der Zande, A. Gijsbertsen, and M. J. J. Vrakking, Phys. Rev. A **76**, 023411 (2007).
[23] NIST Chemistry Webbook: NIST Standard Reference Database Number 69, National Institute of Standards and Technology, http://webbook.nist.gov/chemistry/.
[24] Gerhard Herzberg, *Molecular Spectra and Molecular Structure: Spectra of Diatomic Molecules* (Krieger, Malabar, FL, 1989).
[25] V. Helbig, D. E. Kelleher, and W. L. Wiese, Phys. Rev. A **14**, 1082 (1976).
[26] D. Xiao, C. Cheng, J. Shen, Y. Lan, H. Xie, X. Shu, Y. Meng, J. Li, and P. K. Chu, Phys. Plasma **21**, 053510 (2014).